

Article

Analytic Hierarchy Process (AHP) Based Soil Erosion Susceptibility Mapping in Northwestern Himalayas: A Case Study of Central Kashmir Province

Fayma Mushtaq ^{1,*} , Majid Farooq ¹ , Anamika Shalini Tirkey ²  and Bashir Ahmad Sheikh ¹

¹ Department of Ecology, Environment & Remote Sensing, Government of Jammu and Kashmir, Srinagar 190018, India

² Department of Geoinformatics, School of Natural Resources and Management, Central University of Jharkhand, Brambe, Ranchi 835205, India

* Correspondence: fayma1987@gmail.com

Abstract: The Kashmir Valley is immensely susceptible to soil erosion due to its diverse topography and unstable geological formations in the Himalayan region. The present study helps in assessing the spatial distribution and prioritizing soil erosion zones in the Central Kashmir region covering the Sindh and Dachigam catchments. The study implemented the GIS-based analytic hierarchy process (AHP) and weighted sum method (WSM) using datasets of precipitation, geological map, soil map, and satellite imagery and derived eleven factors (topographical derivatives, LULC, soil, drainage, rainfall, lithology, wetness index and greenness of an area). The ratings and weightage were proven to be unbiased and reliable based on the observed value of the consistency ratio (C_R) (i.e., 0.07). The study depicts 41% of the total area to be extremely vulnerable to soil erosion. The slope varies from 0–62° with mean of 22.12°, indicating 467.99 km² (26%) and 281.12 km² (15%) of the area under high and very high susceptible zones, respectively. The ND_{VI} and ND_{WI} maps indicate soil erosion severity covering an area of 40% and 38%, respectively, in highly susceptible zones. High drainage density and curvature zones were observed in 18.33% and 22.64% of the study area, respectively. The study will assist in the planning and implementation of conservation measures.

Keywords: analytical hierarchy process; pairwise comparison matrix; soil erosion susceptibility; weighted sum method



Citation: Mushtaq, F.; Farooq, M.; Tirkey, A.S.; Sheikh, B.A. Analytic Hierarchy Process (AHP) Based Soil Erosion Susceptibility Mapping in Northwestern Himalayas: A Case Study of Central Kashmir Province. *Conservation* **2023**, *3*, 32–52. <https://doi.org/10.3390/conservation3010003>

Academic Editors: Gowhar Meraj and Svein Øivind Solberg

Received: 29 October 2022

Revised: 17 December 2022

Accepted: 4 January 2023

Published: 7 January 2023



Copyright: © 2023 by the authors. Licensee MDPI, Basel, Switzerland. This article is an open access article distributed under the terms and conditions of the Creative Commons Attribution (CC BY) license (<https://creativecommons.org/licenses/by/4.0/>).

1. Introduction

Soil erosion, a global issue, has a wide range of negative consequences including land deterioration and fertility loss, aside from noticeable off-site repercussions such as the accumulation of sediments, the eutrophication of waterways, and increased flooding [1,2]. Out of all the continents of the world, Asia experiences an excessive rate of erosion of approximately 74-ton acre⁻¹ year⁻¹ [3]. With most of the sediment coming from rivers (with 80% of the total sediments delivered into the world's oceans), the Himalayan rivers are at the foremost, contributing 50% of the overall river sediment flux [4]. The rivers originating in mountainous regions are particularly susceptible to soil erosion, apart from arid, semi-humid, and semi-arid areas [5,6]. The mountainous terrain of the Himalayas is particularly susceptible to severe soil erosion [7] and it alone contributes 25% of the world's sediment load to the oceans [8]. Factors such as climatic dryness, poor soil, and vegetation quality are amongst the many factors causing the deterioration in soil productivity, making an area vulnerable to land degradation [9].

The annual peak of ephemeral streams and rivers in the Himalayas, along with adequate precipitation, causes the easy detachment of soil, resulting in an extremely dissected landscape [10]. Environmentalists and water resource planners are increasingly concerned about the Himalayan ecosystem's fragility. The Himalayas' steep slopes, decreased forest

cover, and strong seismicity have resulted in severe soil loss and consequential increased sediment load in river basins [11]. The Kashmir Valley, in the Western Himalayan region, is unique in itself due to the evolution of its surface features. The valley is situated in a young fold mountain range that still experiences uplifting, resulting in folding, thrusting, faulting, jointing, fissuring, and shearing [12]. The seismic environment, aside from the actions of rivers and glaciers throughout geological time, has made the region imperiled by multiple types of land degradation such as rock falls, rock slides, mud slides, debris fans, and landslides.

For soil erosion assessment, amongst the several techniques, the universal soil loss equation (USLE) is widely used by researchers [13]. The modified equation of USLE is the modified universal soil loss equation (MUSLE) given by Williams [14], followed by the revised universal soil loss equation (RUSLE) given by Renard [15]. There are various other types of models that have been derived from time to time with its own set of traits and application possibilities [16–23] such as the Water Erosion Prediction Project (WEPP) and Soil and Water Assessment Tool (SWAT), to name a few. These methods were implemented by various academics across the sphere to assess the soil erosion rate [24–26].

Although erosion models deliver quantifiable information on soil loss from a specified area, in most instances, the decision-makers and watershed managers are concerned about the erosion hazard spatially, rather than the quantified details of soil loss [27,28]. To weigh the soil loss risk, diverse methodologies such as multi-criteria evaluation based on ranking are employed with the spatial assessment of erosion risk based on various environmental conditions. The advancement in remote sensing and geographical information system (GIS) has assisted researchers in exploring the geographical distribution patterns of soil deterioration, providing a better understanding of erosion-inducing components such as topography by combining RS, digital terrain modeling (DTM), and GIS [28–30] and in implementing sustainable land and soil conservation techniques [31]. Furthermore, the soil loss hazard map points toward the spatial extent and severity of loss, which can be used in strategic policy decisions [32]. One of the most extensively used method for soil susceptibility mapping is the analytic hierarchy process (AHP), established by a methodical decision-making procedure to improve solutions for issues with numerous criteria (e.g., soil erosion risk assessment with very high efficacy) [33–39]. The method has been commonly used across the globe to provide a framework for the identification of the highest priority areas for soil conservation measures and sustainable management [40–43].

The other techniques employed for mapping soil erosion includes frequency ratio (FR), weights-of-evidence (WoE), logistic regression (LR), and ANN [44]. Researchers have employed ANN in a GIS environment for soil erosion studies [45,46], but the need for sufficient data in ANN analyses is seen as a potential limitation [47], and where the test data include values outside the training data range, weak predictions may occur [48]. In addition, the fuzzy relations technique has been used to map the susceptibility of soil erosion in Taebaek city (which belongs to the Samcheok Coalfield), Korea by [49]. However, the lack of a systematic and effective design is seen as a weakness of the fuzzy operator method [50].

A variety of statistical and advanced methods such as the evidential belief function (EBF), WoE, and adaptive neuro-fuzzy inference system have been applied and tested in the fields of flooding and landslide; however, they have not been attempted in soil erosion modeling [51]. Over a period of time, there has been much advancement in the field of modeling through artificial intelligence, but the absence of soil erosion data and other watershed information limits the results of soil-erosion modeling. A meagre number of indicators and a lack of assessment methods are major disadvantages to the use of empirical soil erosion models. In order to overcome these disadvantages, a new approach that integrates empirical and artificial intelligence modeling procedures has improved the identification of soil erosion hot spots, especially in watersheds lacking soil erosion data. More recently, hybrid/ensemble models have been developed in a combined way via an integration of individual machine learning (ML) models and statistical approaches. The usefulness of the

hybrid models that have been discussed in various publications [52,53] lies in their highest accuracies in comparison to individual models [54,55]. Although these ML techniques have been employed in the past, they have only been used infrequently for erosion modeling as the computing costs are higher and needs a high level of handling expertise. Based on the literature review, the complexity and time required for the analysis are the major limitations of the current methods. Thus, the simplicity, comparative accuracy, and GIS compatibility of the statistical methods have been seen to become one of the more frequent geo-hazard analytical techniques [56]. Moreover, its performance is rapid and the output accuracy is high [57]. Furthermore, as reported by [49], the statistical method produces a more precise measure of the success rate than the ANN and probabilistic methods.

The Kashmir Valley is immensely susceptible to soil erosion due to its diverse topography with most of its land subjected to various types of soil erosion due to weak and unstable geological formations [58]. The combined effect of all of these factors makes the region susceptible to erosion, ultimately depleting the soil fertility, productivity, and deterioration of water bodies [24]. It is important to thoroughly understand the pattern of soil erosion susceptibility to developing better erosion management practices, improved land use policies, and the efficient management of natural resources for the rehabilitation of the degraded land. As there has not been sufficient research in the study area, we evaluated various factors in the process of soil erosion in the catchments of the Sindh and Dachigam watersheds, which is not well-understood and needs attention.

The present study was carried out over the entire catchments of Sind and Dachigam in Central Kashmir Province using a combination of GIS, remote sensing data, and AHP models to assess the soil erosion susceptibility. The study attempted to answer some specific questions such as what is the spatial distribution pattern of the soil erosion severity zones and what are the prioritized zones of soil erosion risk for the planning and implementation of conservation measures? This study explains a simple and inexpensive aid tool for modeling and mapping the areas susceptible to soil erosion, especially for inaccessible areas where field measurements are rare or even non-existent.

2. Study Area

The Central Kashmir region covering the Sindh and Dachigam catchments lies between 34°00'56.49" N to 34°27'46.45" N latitude and 74°36'44.98" E to 75°29'56.58" E longitude (Figure 1). It is located at 1585 m amsl, on the banks of the Jhelum River. Srinagar city lies in the midst of the rock depression of the Valley of Kashmir, about 35 km in breadth and 160 km in length. The physiographic setting of Srinagar city is characterized by low lying agricultural fields in the southern and western sides of floodplains of the Jhelum River. It has steep hills in the east and northeast, the famous Karewas Hills (locally called as Wudars) in the far southeast, and small hills in the northern area. Similarly, in the east lies the Basiwan, Zabarwan, and Dachigam Hills along with the famous Dal Lake on the foothills. The climate in the region is sub-Mediterranean with cold winters (December–February) and warm summers (June–August). The coldest (January) and warmest (July) months have the average temperature of 3.5 °C and 30 °C, respectively. Winter is very cold and from the last week of December to the first week of March, the temperature is often subzero. The mean annual precipitation is around 660 mm year⁻¹ and a significant amount of precipitation occurs in the form of snow. Relative humidity was the maximum in the month of January (i.e., 85%) and it is minimum in the month of June (about 57%). The area comes under the Western Himalayan Region: Agro-climatic Zone-I.

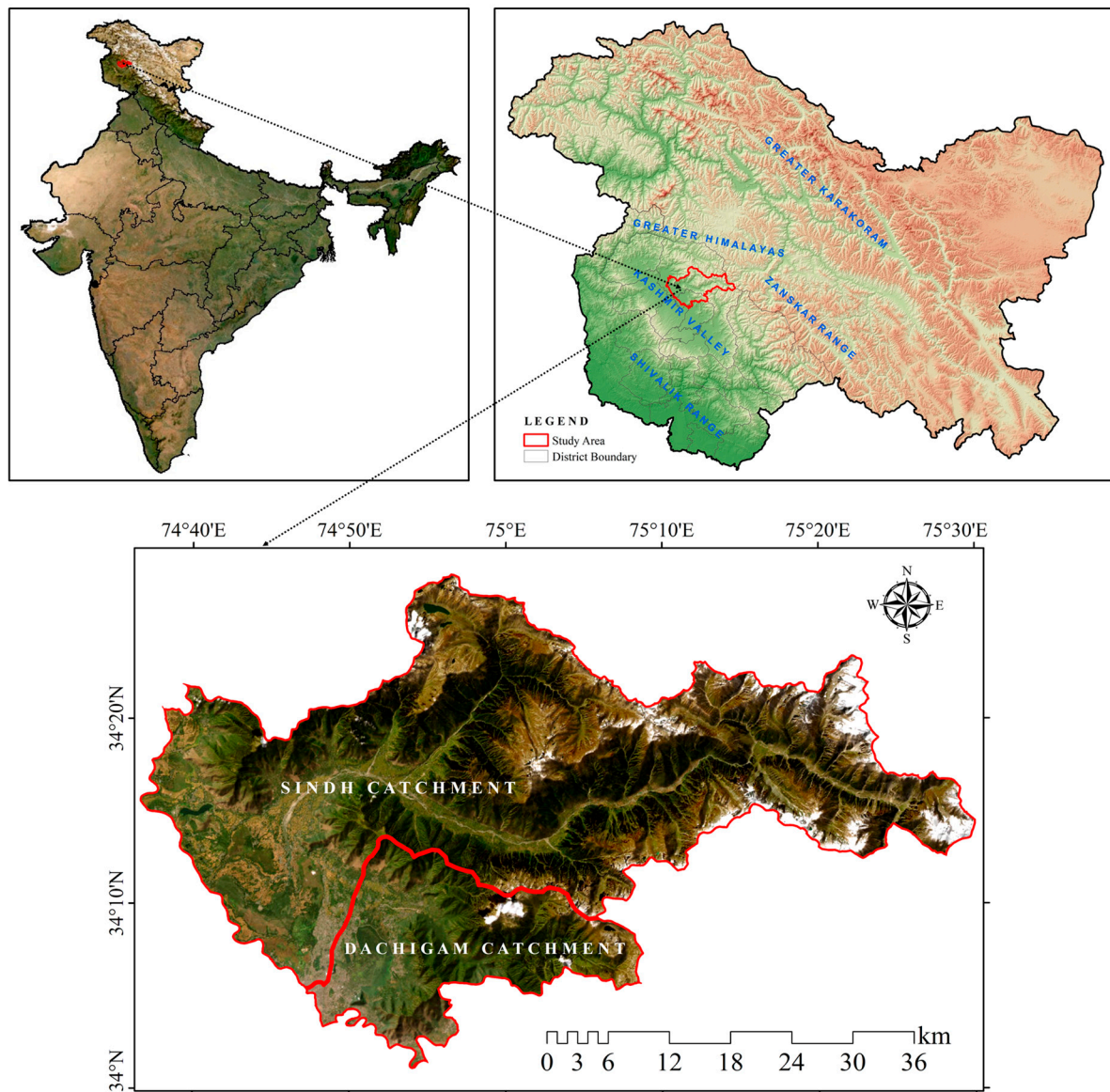


Figure 1. Location map of the Central Kashmir region.

3. Materials and Methods

For soil erosion susceptibility modeling, it is vital to prepare and investigate the impact of different factors that affects the erosion [59]. In the present study, different types and sources of data were used: satellite data, digital elevation model, geological data, soil data, and meteorological data. The basic datasets used includes: Shuttle Radar Topographic Mission (SRTM) Digital Elevation Model (DEM) (30 m resolution), Satellite imagery from Cartosat 1B (2.5 m resolution), Indian Remote Sensing (IRS) Linear Imaging Self Scanning (LISS)-III (23.5 m resolution), and Landsat 8 Operational Land Imager (OLI) (30 m resolution), daily rainfall data of the Indian Meteorological Department (IMD) from (1980–2017). The SRTM DEM and Landsat 8 OLI satellite imagery were obtained from the USGS Earth Explorer data portal (<https://earthexplorer.usgs.gov/>) accessed on 15 November 2020. The Cartosat 1B and IRS-LISS III satellite imagery were procured from National Remote Sensing Center, ISRO's EO data hub (<https://bhoonidhi.nrsc.gov.in>) accessed on 24 October 2020. The historical rainfall data of Srinagar Station were obtained from the Indian Meteorological Department Met Center Srinagar (<https://mausam.imd.gov.in/srinagar/>) accessed on 19 November 2020. The remote sensing data of Cartosat 1B, IRS-LISS III were used for the preparation of land use/land cover, lithology, and soil

layers. The SRTM DEM data were used for the derivation of topographical parameters and drainage of the study area. The Landsat-8 OLI satellite image was used for the generation of water and vegetation indices and the rainfall data of Srinagar Station was used for the calculation of the rainfall erosivity factor. Table 1 presents the sources of the datasets and procedures employed for the generation of various derivatives. For the analysis, all datasets were projected into a common projection system (i.e., Universal Transverse Mercator (UTM)) and resampling was conducted using the nearest neighbor technique. The overall methodology adopted for soil erosion susceptibility modeling is given in Figure 2.

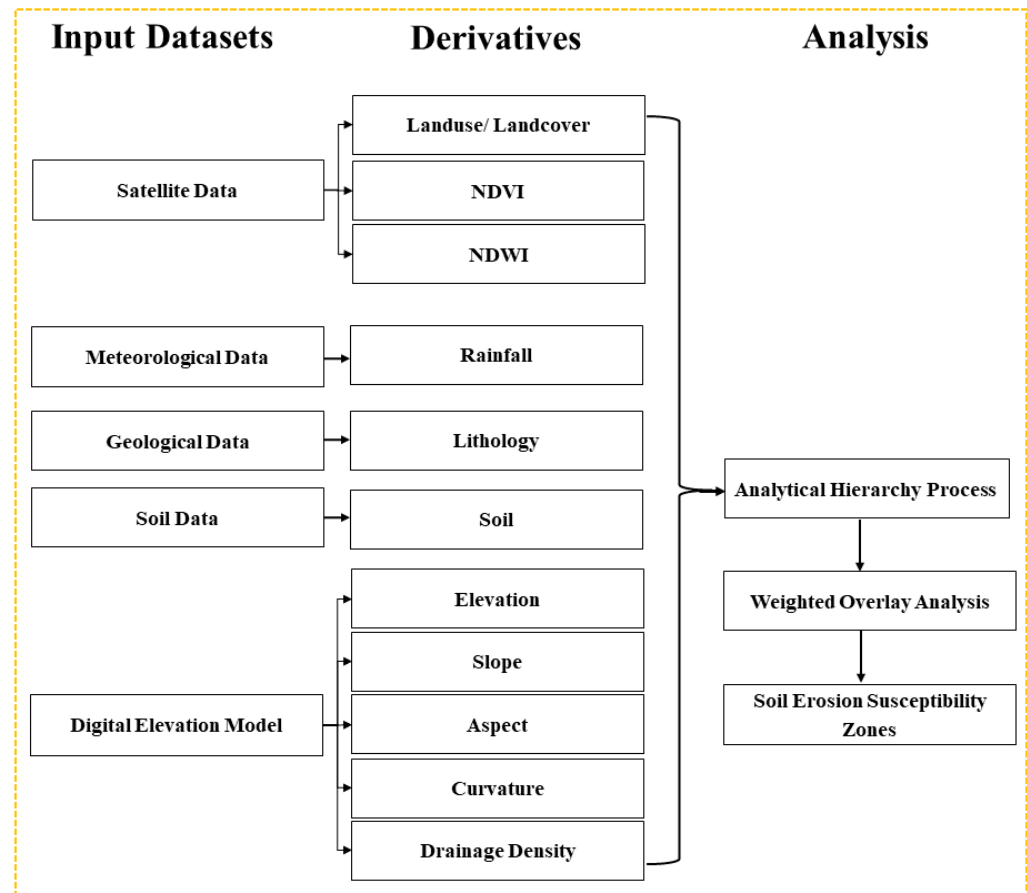


Figure 2. Flowchart of the methodology adopted.

3.1. Soil Erosion Conditioning Parameters

Based on the understanding, experience of an area, and the evaluation of the data generated based on a review of the published literature, eleven influencing factors (elevation, slope, aspect, curvature, soil, land use/cover, drainage density, rainfall erosivity, lithology, NDWI, and NDVI) were selected for analysis in the Sind and Dachigam catchments [34,60–63]. The rationale behind selecting each of the eleven parameters and the procedures to generate them is discussed below:

Elevation (E_L): Elevation is one of the main components that affects the rate of erosion as a function of its impact on soil moisture and water balance, erosional and depositional processes, soil organic matter, biomass, and species production of cultivated plants and natural flora [61]. The elevation layer obtained from SRTM DEM was subjected to the classification in order to use as the input in the overlay analysis (Figure 3a).

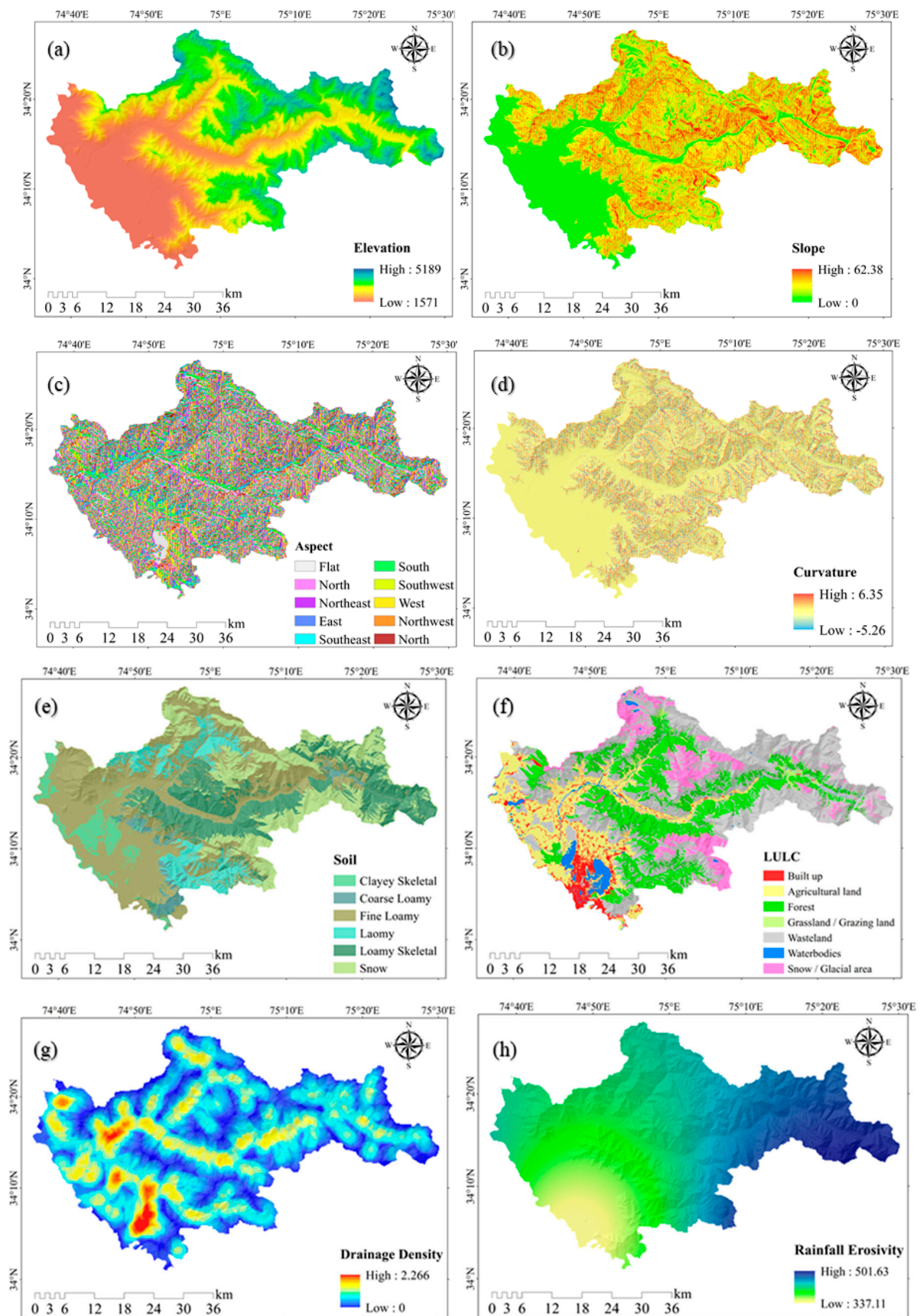


Figure 3. Parameters considered for the estimation of soil erosion severity. (a) Elevation, (b) Slope, (c) Aspect, (d) Curvature, (e) Soil, (f) LULC, (g) Drainage Density, (h) Rainfall Erosivity.

Slope (S_L): The runoff velocity and infiltration rate are dependent on the slope angles. High runoff velocity in steep sloped areas increases the erosion rates compared to low angle slopes where the infiltration rate is high. To measure the impact of the gradient on erosion, a slope map in degrees was generated in ArcGIS using SRTM DEM for the study area (Figure 3b).

Aspect (A_S): The direction of slope can be determined using aspect, a crucial factor in erosion. For example, north-facing slopes have lower risks of erosion than south-facing slopes. The slope direction was categorized in nine classes such as flat, north, northeast, east, southeast, south, west, southwest, and northwest (Figure 3c).

Curvature (C_U): The degree to which a curve diverges from its straight path is defined by curvature, which affects the divergence and convergence toward downward flow with respect to slope [64]. This layer was derived using SRTM DEM using proximity analysis (Figure 3d).

Soil (S_O): Soil type exhibits susceptibility to soil erosion and is directly regulated by characteristics such as texture, organic matter content, parent material, porosity, structure, and infiltration potential [65]. The soil layer was created after executing selective ground truthing using the soil texture map of the Indian Soil and Land Use Survey created by the J&K Remote Sensing Center of Srinagar using IRS-LISS III data (Figure 3e).

Land Use/Land Cover (LU_{LC}): LU_{LC} plays a vital role in many hydrological processes such as infiltration, runoff velocity, evapotranspiration, and soil erosion [66]. The LU_{LC} map was derived from Cartosat 1B data (2.5 m resolution) using on screen digitization and selective ground truthing. The validation of LU_{LC} using the Cohen's Kappa index test indicated 89% accuracy (Figure 3f).

Drainage Density (D_D): The drainage network is a significant variable that affects the erosion in mountainous areas by eroding the sediment deposits, carrying and depositing them to water bodies [67]. Dense areas mean a large number of streams and therefore a high probability of soil erosion. The drainage network was delineated from the DEM (Figure 3g).

Rainfall Erosivity (R_E): This is an influential factor defined as the potential of rainfall to trigger soil loss from hill slopes by the action of water. The characteristics of precipitation such as volume, magnitude, and seasonal distribution also affects erosion [68]. Due to the inaccessibility of high-resolution precipitation databases for the area, it was considered as an extensively challenging task to calculate these parameters. In such situations, numerous empirical models were employed for the calculation of rainfall from the daily precipitation data [69]. The relationship developed by [70] and used by [71–73] was used to evaluate the rainfall erosivity factor (Figure 3h).

Lithology (L_I): The lithological condition is an important component controlling erosional processes. Lithological properties affect the nature of alluvial undulations, slopes, soil types, raw materials, and sediments. The lithofacies were generated by the J&K Remote Sensing Center of Srinagar using IRS-LISS III data (Figure 3).

Normalized Difference Water Index (ND_{WI}): This represents the water content of the vegetation, defined as the ratio of the erosion intensity of water flow, presuming that the rate of flow is adequate to a specific area [74]. This is often a function of the regional climate and soil characteristic that controls the water availability [75,76]. The index is calculated by the ratios of the green and NIR bands of the OLI satellite data (Figure 3).

Table 1. Data sources and techniques used for the preparation of thematic data layers.

S. No.	Parameter	Source	Procedures	Reference
1.	E_L	SRTM DEM	30 × 30 m DEM	[77]
2	S_L	SRTM DEM	$\tan \theta \frac{N \times i}{636.6} = \text{no of contour cutting};$ $i = \text{contour interval}$	[78]
3	A_S	SRTM DEM	$= 1 - \sqrt{2} \left(\frac{b}{k\delta} \right) \frac{A_S(p, q)}{\sqrt{1 + q + q^2 / (1 - p + q)}}$	[79]
4	C_U	SRTM DEM	$CU = II \frac{dT}{ds} II$	[80]
5	S_O	SLUSI	On screen digitization	[81]
6	LU_{LC}	IRS LISS-IV	On screen digitization	[82]
7	D_D	SRTM DEM	Proximity analysis	[83]
8	R_E	IMD	$RE = 79 + 0.363R$	[71]
9	L_I	NRIS	On screen digitization	[84]
10	ND_{WI}	LANDSAT	$NDWI = \frac{(Green - NIR)}{(Green + NIR)}$	[85]
11	ND_{VI}	LANDSAT	$NDVI = \frac{(NIR - Red)}{(NIR + Red)}$	[86]

Normalized Difference Vegetation Index (ND_{VI}): Vegetation cover is one of the key aspects and is close to the terrain that controls the risk of soil loss [87]. As it rains over vegetation, their canopy blocks the rain, which reduces the impact of raindrops and increases infiltration [87]. In general, ND_{VI} is inversely proportional to soil erosion. For example, when forests exceed 20–35% of the area, wind erosion is significantly reduced [88]. The ND_{VI} was derived by using red and NIR bands of the Landsat 8 OLI satellite data (Figure 3).

3.2. Determination of Weights by the AHP Procedure

The analytic hierarchy process (AHP), also known as the Saaty method, is a semi-quantitative, multipurpose, multi-criteria technique commonly employed in modeling the risk of soil erosion [34,37,39,78]. AHP is applied for decision-making, in which problems are split into several parameters, arranged in a hierarchical structure followed by evaluation of the relative significance of each pair of element, and the final integration of results [89]. There are five or more classes at each theme level, signifying that the relationships between these related classes are too intricate. Therefore, the relationships between the 11 subject levels were derived with the help of AHP through widespread applicability in decision-making, vulnerability analysis, and planning [90]. The method for deriving different subject layer weights using AHP involves the following steps:

- Development of the spatial database;
- Establishment of evaluation criteria and hierarchical structure for multi-criteria questions;
- Use the AHP method to compute the weight of the relative importance of the criteria;
- Finally, the weighted sum method (WSM) is employed to estimate the severity of soil erosion.

Databases for multiple theme layers were generated in the ArcGIS environment. The 11 parameters mentioned in Section 3.3 were chosen as the evaluation criteria and prioritized based on the literature research, knowledge, and collective opinion of experts. The combined judgement helped to rank the parameters by the most important criterion, which may trigger soil loss. To generate a paired comparison matrix (PCM), the relative importance of values was decided based on Saaty's scale of 1 to 9 where 1 and 9 denote equal importance between the two factors and extreme importance of one factor in comparison to the other, respectively [91] (Table 2).

Table 2. Continuous rating scale for a pairwise comparison of Saaty’s method [91].

Intensity of Importance	Definition
1	Equal Importance
3	Moderate Importance
5	Strong Importance
7	Very Strong Importance
9	Extreme Importance

After creating a pairwise comparison matrix using the preference values, the matrix was analyzed to find the performance ratings of each of these criteria in achieving the related weights, and the consistency property of the matrix was then verified to ensure the consistency of judgements in the PCM. The AHP apprehends the information of ambiguity in judgements by means of the principal eigen value and the consistency index [92]. Saaty provided a measure of consistency, termed the consistency index (C_I), which is the deviation or degree of consistency derived by Equation (1), given below as.

$$C_I = \frac{(\lambda_{max} - n)}{n - 1} \tag{1}$$

where λ_{max} is the highest eigenvalue of PCM and n is the number of classes. Consistency ratio (C_R) is the degree of consistency of PCM, as shown by Equation (2).

$$C_R = \frac{C_I}{R_I} \tag{2}$$

where R_I is the ratio index. If $C_R \leq 0.1$, the inconsistency is acceptable. If $C_R > 10\%$, subjective judgment needs to be revised.

3.3. Weighted Sum Method (WSM)

For the implementation of WSM, all selected factors were reclassified in five priority classes as very low, low, medium, high, and very high (Table 3). The class range was derived from each raster layer after reclassification. The natural break classification was used in ArcGIS to optimize the arrangement of a set of values into “natural” classes. Five priority classes were used based on the available literature [73,93–98]. Within each layer, a rating from very low (1) to very high (5) was assigned to the classes in increasing order of their qualitative importance for erosion [99]. The rankings were assigned to each parameter and their respective classes were dependent upon the functional relationship with soil erosion severity. Higher scale values were assigned to cells that are very highly prone to soil erosion, and lower values were given to cells that are less prone to erosion. Finally, the soil erosion severity was determined on a pixel basis using a WSM. In the WSM, each parameter under consideration was multiplied with its respective weight and the summation of all the layers resulted in a soil severity index.

$$SES = E_{Lw} \times E_{Lwj} + S_{Lw} \times S_{Lwj} + A_{Sw} \times A_{Swj} + C_{Uw} \times C_{Uwj} + S_{Ow} \times S_{Owj} + LU_{LCw} \times LU_{LCwj} + D_{Dw} \times D_{Dwj} + R_{Ew} \times R_{Ewj} + L_{Iw} \times L_{Iwj} + ND_{WIw} \times ND_{WIwj} + ND_{VIw} \times ND_{VIwj} \tag{3}$$

where SES shows the areas of soil erosion severity. $E_L, S_L, A_S, C_U, S_O, L_U, D_D, R_E, L_I, ND_{WI}$, and ND_{VI} represent the layers of elevation, slope, aspect, curvature, soil, LULC, drainage density, rainfall erosivity, lithology, NDVI, and NDWI. The weight of a layer and of a particular parameter is represented by w and wj .

Table 3. Scale value assigned to different thematic layers as per the soil erosion severity.

S. No.	Thematic Layers	Classes	Scale Value	Soil Severity
1	E_L (m)	1571–2001	1	Very Low
		2001–2659	2	Low
		2659–3298	3	Medium
		3298–3906	4	High
		3906–5189	5	Very High
2	S_L (degrees)	0–8	1	Very Low
		8–20	2	Low
		20–30	3	Medium
		30–38	4	High
		38–62	5	Very High
3	A_S	–1–68	1	Very Low
		68–143	2	Low
		143–217	3	Medium
		217–289	4	High
		289–359	5	Very High
4	C_U	–5.26–0.98	1	Very Low
		–0.98–0.30	2	Low
		–0.30–0.25	3	Medium
		0.25–0.98	4	High
		0.98–6.35	5	Very High
5	S_O	Coarse Loamy	1	Very Low
		Fine Loamy/Clayey Skeletal	2	Low
		Loamy Skeletal/Loamy	3	Medium
6	LU_{LC}	Snow/Glacial area	1	Very Low
		Waterbodies	1	Very Low
		Built-up	2	Low
		Forest	2	Low
		Agricultural land	3	Medium
		Grassland/Grazing Land	4	High
		Wasteland	5	Very High
7	D_D	0–0.28	1	Very Low
		0.28–0.56	2	Low
		0.56–0.86	3	Medium
		0.86–1.29	4	High
		1.29–2.27	5	Very High
8	R_E	337.12–375.18	1	Very Low
		375.18–406.80	2	Low
		406.80–435.19	3	Medium
		435.19–464.86	4	High
		464.86–501.64	5	Very High

Table 3. Cont.

S. No.	Thematic Layers	Classes	Scale Value	Soil Severity
9	L_I	Waterbody Mask	1	Very Low
		Massive Granite Plutonic Rocks/Amygdaloidal basalt	2	Low
		Phyllites Schists	3	Medium
		Slates/Quartzite Shale		
		Phyllite Beds	4	High
Sandstone and Conglomerate/Sandstone/Claystone/Siltstone	5	Very High		
10	ND_{WI}	−0.98–0.24	1	Very Low
		−0.24–0.19	2	Low
		−0.19–0.13	3	Medium
		−0.13–0.07	4	High
		−0.07–0.16	5	Very High
11	ND_{VI}	−0.10–0.06	5	Very High
		0.06–0.12	4	High
		0.12–0.18	3	Medium
		0.18–0.24	2	Low
		0.24–1.0	1	Very Low

4. Results and Discussion

As stated in the Methods section, the PCM was used to compute the criteria weights for each parameter using the AHP methodology. The rankings were decided on the basis of local knowledge of the area under consideration and the literature [37,73,93,95–98]. The ratings and weightage used in this study were proven to be unbiased and reliable based on the observed value of $C_R = 0.07$ in PCM (Table 4), which was in uniformity with the results obtained by [100]. Jaiswal et al. [101] obtained a consistency ratio of 0.093 or 9.3% and concluded that in the case of CR being less than 10%, inconsistency in the decision was acceptable and the weights obtained could be used for priority assessment. The soil erosion severity calculated on the pixel basis was the result of Equation (4), as given below.

$$SES = E_{Lw} \times 0.243 + S_{Lw} \times 0.179 + A_{Sw} \times 0.143 + C_{Uw} \times 0.112 + S_{Ow} \times 0.089 + LU_{LCw} \times 0.068 + D_{Dw} \times 0.053 + R_{Ew} \times 0.039 + L_{Iw} \times 0.030 + ND_{WIw} \times 0.024 + ND_{VIw} \times 0.018 \quad (4)$$

Table 4. Pairwise comparison matrix.

	E_L	S_L	A_S	C_U	S_O	LU_{LC}	D_D	R_E	L_I	ND_{WI}	ND_{VI}
E_L	1	1	3	3	7	5	5	7	7	9	5
S_L	1	1	3	2	3	4	5	5	4	3	3
A_S	0.33	1	1	3	2	3	4	5	5	4	3
C_U	0.33	0.33	1	1	3	2	3	4	5	5	4
S_O	0.14	0.33	0.33	1	1	3	2	3	4	5	5
LU_{LC}	0.2	0.14	0.33	0.33	1	1	3	2	3	4	5

Table 4. *Cont.*

	E_L	S_L	A_S	C_U	S_O	LU_{LC}	D_D	R_E	L_I	ND_{WI}	ND_{VI}
D_D	0.2	0.2	0.14	0.33	0.33	1	1	3	2	3	4
R_E	0.14	0.2	0.2	0.14	0.33	0.33	1	1	3	2	3
L_I	0.14	0.14	0.2	0.2	0.14	0.33	0.33	1	1	3	2
ND_{WI}	0.11	0.14	0.14	0.2	0.2	0.14	0.33	0.33	1	1	3
ND_{VI}	0.2	0.11	0.14	0.14	0.2	0.2	0.14	0.33	0.33	1	1
<i>Sum</i>	3.79	4.59	9.48	11.34	18.2	20	24.8	31.66	35.33	40	38
C_R	0.07										

4.1. Soil Erosion Susceptibility Classes

The final map of soil erosion susceptibility for Central Kashmir prepared using the GIS-based approach is given in Figure 4. Based on the severity of soil erosion, the derived layer was classified into five classes based on natural break classification as very low, low, medium, high, and very high (Table 5). It was observed that 15% (275.14 km²) and 19% (345.85 km²) of the area came under very low to low levels of erosion severity, located at relatively lower elevations (1571–2659 m), mostly including valley floors where the majority of the land use is agriculture and built-up. In addition, the low values can be associated with the soil texture, which is predominantly fine loamy to loam at lower elevations because the susceptibility of soil to erosion agents is closely related to the soil physical, chemical, and biological properties [102,103]. The particle size directly influences erosion in many ways [104–108]. In essence, sand, sandy loam, and loamy soils are less erodible than silt, very fine sand, and certain clayey soils [109]. The medium susceptible class covered an area of 25% (465.08 km²), mostly associated with the forest cover. The forest provides good protection against surface runoff and soil erosion losses [110], despite the fact that it comes under the moderate category due to the fact that the majority of forest area is under steep slopes and at higher elevations compared to the agriculture and built-up area, which are under relatively less steep slopes and at lower elevations. This may be the reason for the comparatively high soil erosion severity by forest land use compared to other land uses. Overall, 41% (741.65 km²) of the region was highly susceptible to erosion comprising high and very high susceptible zones. These regions are situated at very high elevation (3298–5189 m), mostly comprising the wasteland category. The occurrence of steep slopes and the presence of more erodible soil particles confers higher soil loss susceptibility. The undulating topography with steeper slopes accompanied with heavy rainfall in the Himalayan region is predisposed to natural hazards including soil erosion [111].

Table 5. Classes according to susceptibility to erosion.

Very Low		Low		Medium		High		Very High	
Area (km ²)	Percentage (%)								
275.14	15%	347.85	19%	465.08	25%	491.40	27%	250.25	14%

4.2. Soil Erosion Influencing Parameters

The quantitative and qualitative results of the vulnerability of soil erosion obtained through zonal statistics are presented in Tables 6 and 7.

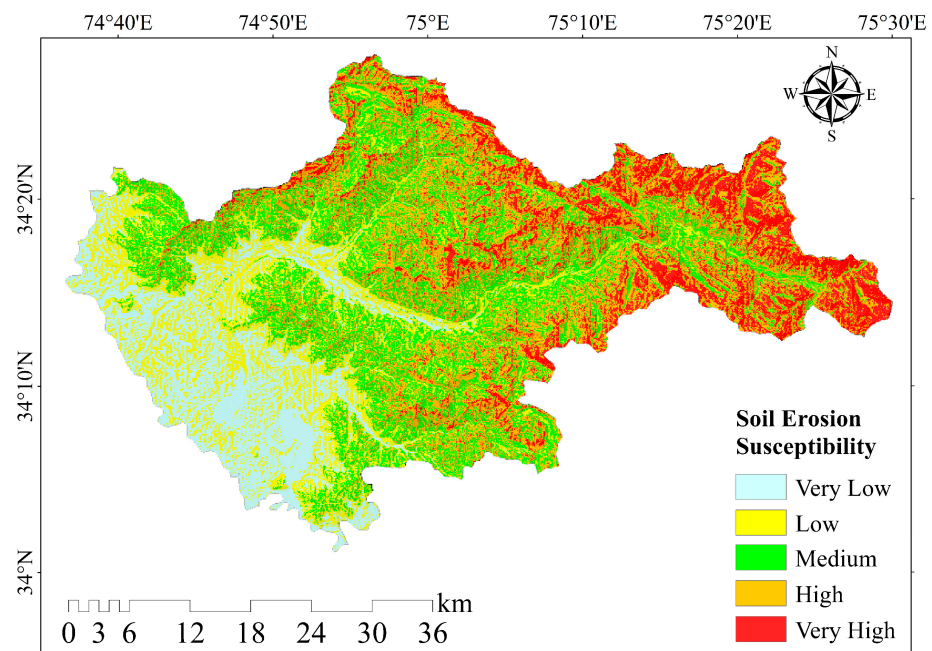


Figure 4. Soil erosion severity map of the Central Kashmir region.

Table 6. Percentage distribution of elevation, slope, aspect, curvature, and rainfall.

Soil Erosion Susceptibility Class	Area Coverage (km ²) and Percentage (%)											
	<i>E_L</i>		<i>S_L</i>		<i>A_S</i>		<i>C_U</i>		<i>D_D</i>		<i>R_E</i>	
	km ²	%	km ²	%	km ²	%	km ²	%	km ²	%	km ²	%
Very Low	499.44	27%	412.74	23%	339.82	19%	96.26	5%	502.41	27%	266.51	15%
Low	309.87	17%	271.50	15%	376.93	21%	364.26	20%	534.17	29%	382.06	21%
Medium	348.78	19%	396.37	22%	392.58	21%	969.68	53%	457.93	25%	544.87	30%
High	403.87	22%	467.99	26%	381.03	21%	314.65	17%	278.50	15%	299.76	16%
Very High	267.76	15%	281.12	15%	339.35	19%	84.87	5%	56.71	3%	336.51	18%
Total Area	1829.72											

Table 7. Percentage distribution of LULC, lithology, NDVI, NDWI, and soil.

Soil Erosion Susceptibility Class	Area Coverage (km ²) and Percentage (%)									
	<i>LU_{LC}</i>		<i>L_I</i>		<i>ND_{VI}</i>		<i>ND_{WI}</i>		<i>S_O</i>	
	km ²	%	km ²	%	km ²	%	km ²	%	km ²	%
Very Low	220.42	12%	15.57	1%	157.44	9%	160.03	9%	510.10	28%
Low	525.61	29%	181.17	10%	407.74	22%	441.33	24%	742.33	41%
Medium	286.08	16%	558.13	31%	531.08	29%	521.09	28%	577.29	32%
High	30.73	2%	488.30	27%	441.58	24%	427.22	23%	-	-
Very High	766.87	42%	586.54	32%	291.87	16%	280.04	15%	-	-
Total Area	1829.72									

Elevation is a substantial factor that affects the soil erosion in mountainous regions [34]. Elevation influences the distribution of plant growth, physiography, and morphology [112]. The elevation ranges from 1571 to 5189 m with a mean of 2842.94 m. Out of the total

study area, 27.53% is under an elevation range of 1571–2001 m. The elevation ranges of 3298–3906 m and 3906–5189 m covered 21% and 15% of the study area, respectively. The soil erosion severity associated with elevation showed that 37% of the area fell under the high to very high-risk zones comprising 403.87 km² and 267.76 km², respectively. The higher elevation zones contributed more to soil erosion [61] while the very low (499.44 km²) to low (309.87 km²) zones comprised 44% (499.44 km²), and the medium zone covered 19% (348.78 km²).

Slope gradient is the foremost factor that can lead to soil loss subjected to the degree of steepness [113]. The slope varies from 0–62° with a maximum area of 25.84% under a slope range of 30–38°, followed by 21.96% under 20–30°. The mean slope observed was 22.12° with a standard deviation of 13.94°. The distribution of the slope gradient indicates that 467.99 km² (26%) of the area was highly susceptible; 281.12 km² (15%) was very highly susceptible; medium was 396.37 km² (22%), and very low (412.74 km² to low 271.50 km²) was 38%. The higher slope values may be attributed to the abrupt slope variations near the drainage channels and the highly dissected topography. The higher slope in the region corresponds to the high mountain–deep valley type of geomorphology. Areas exhibiting higher slope values are highly vulnerable to soil erosion due to the impact on runoff velocity and associated material removal. The greater accumulation of runoff on longer slopes of the terrain increases its detachment and transport capacities [70]. In general, the steeper the slope of the land, the greater the amount of soil loss by water will be. Soil erosion by water accelerates as the slope length increases due to a greater accumulation of runoff. Often, the consolidation of small fields by removing the field boundaries into a larger one results in longer slope lengths that will increase the erosion potential due to the increased velocity of water [114].

Aspect plays a critical role in influencing the vegetation pattern, and hence erosion [115]. Aspect is another essential factor in soil erosion estimation as it also influences the period of sunlight, type of greenness, wetness, and water loss [116]. Moreover, the slope aspect can interact with other environmental variables (e.g., slope position) to jointly influence the vegetation structure [117,118]. The percentage of aspect distribution that was highly susceptible covered an area of 720.38 km² (40%), confined to the aspect range of 217–359, which covered 39.40% of the study area. The zones that were the least and medium susceptible covered an area of 716.75 km² and 392.58 km², respectively.

The stream density and watershed morphology are robustly influenced by the curvature of the hill slope. The vulnerability of the landform components to erosion varies depending on the gradient of the hill slope, Planform curvature, and profile curvature [61,65]. The distribution of the curvature layer indicates that the maximum of the area was occupied in the medium zone (i.e., 969.68 km² (53%)), followed by low (364.26 km² (20%)), and high zones (314.65 km² (17%)). The medium curvature zone covered 54.35% of the study area, followed by a low zone of 23.01%. Only 17.75% and 4.89% of the study area were under high curvature zones.

Drainage density, like other parameters, is an index of soil erosion [39]. Explicitly, drainage densities greater than the threshold of 0.9 km/km² have been found to be linked to high risks of soil loss [10]. The susceptibility zonation showed that 502.41 km² (27%) and 534.17 km² (29%) of the area came under very low to low zones followed by the medium class 457.93 km² (25%), high 278.50 km² (15%), and very high 56.71 km² (3%). This is due to the fact that the majority of the area is under low drainage density zones (0–0.56) comprising 56.58% of the study area. The range from 0.56 to 0.86 comprised 25.09% of the study area. Only 18.33% of the area is under high drainage density. The area with a greater density signifies a greater number of streams, and thereby a higher possible rate of soil erosion. The drainage network influences the soil erosion process by eroding and transporting the sediments through streams, and is an important variable influencing soil erosion processes in mountainous regions [67].

Rainfall is an imperative factor that leads to soil loss due to the influence of raindrop and its capacity to take away the soil masses downslope [10]. The increase in rainfall

amount has a significant impact on soil erosion depending on the type, duration, and extremeness in a particular season or year [119]. The rainfall erosivity index was extracted using the technique given in Table 1. The rainfall erosivity in the study area ranges from 337.18–501.64 MJ/mm/ha/h/yr with a mean and standard deviation of 421.39 and 40.19 MJ/mm/ha/h/yr, respectively. The rainfall erosivity distribution showed that 30% (544.87 km²) of the area was under the medium zone, followed by the very low 21% (382.06 km²), and very high 18% (336.51 km²). The rainfall erosivity values increased from the alluvial plain region with the lowest elevation in the south/southwest part of the study area toward the hilly areas in the northeast direction. George et al. [120] worked in Uttarakhand State and reported a similar type of variation in the rainfall erosivity factor with an increase in the alluvial/tarai plain region with the lowest elevation toward the Shivalik Hills region.

The hydrological and geomorphic behavior of any landscape is affected by the type of LU_{LC} [121]. The extent to which the soil can be eroded is controlled by the proportion of vegetation cover existing in an area [113]. Less vegetation cover exposes the soil to erosion through the impact of precipitation and surface runoff [122]. The different land cover classes have different rates of soil moisture, infiltration, evapo-transpiration, and interception process [123]. The percent distribution of LU_{LC} and sensitivity to erosion classes in the Central Kashmir region is presented in Table 7. The results indicated that 797.6 km² (44%) of the land use was highly susceptible; 286.08 km² (16%) was moderately sensitive, and 746.03 km² (41%) was the least sensitive to erosion. The higher percentage of susceptibility to erosion was due to less plant cover in the study area, because a major portion of the catchment was under the wasteland category, covering 40.60% of the total study area. The moderately sensitive zone came under forest cover, covering 24.50% of the study area followed by agricultural land (i.e., 16%) because forest areas are generally known for their ability to control soil erosion [124]. The rates of erosion are effectively slowed down by means of a higher percentage of plant cover and large amounts of root biomass [125]. The tree canopies and the foliage of smaller plants intercept the rain water and thus also help in preventing erosion [126].

Lithology demonstrates the overall physical properties of rocks, comprising primarily igneous, sedimentary, and metamorphic rocks, which have a specific behavior to soil erosion [34]. From the lithological map, it can be perceived that the majority of the area is under sand/silt with clay comprising 32.91% of total study area, followed by sandstone and conglomerate/sandstone/claystone/siltstone with an area of 25.63%, and 29.09% of the area is under phyllites schists slates/quartzite shale phyllite beds. The classification of the lithology showed that only 196.74 km² (11%) of the region was least sensitive to soil erosion. The maximum of the area was either moderately sensitive 558.13 km² (31%), high 488.30 km² (27%), and very highly 586.54 km² (32%) sensitive to erosion.

ND_{VI} exhibits greenness and vegetation health [127]. The mean ND_{VI} values obtained were 0.14 with a standard deviation of 0.07. Good vegetation cover such as dense forested areas with positive ND_{VI} values diminishes the possibility of erosion while barren areas with near zero ND_{VI} values have a greater susceptibility to erosion. On the other hand, ND_{WI} estimates the rate of erosion based on the wetness of soil along with its depth [34]. Areas with higher values of ND_{WI} greatly influence the erosional processes [128]. The mean and standard deviation of ND_{WI} obtained were -0.15 and 0.07 , respectively. The reclassified maps of ND_{VI} and ND_{WI} indicated an overall similar distribution in terms of soil erosion severity covering an area of 733.45 km² (40%) and 707.26 km² (38%), respectively, in highly susceptible zones.

The type of soil impacts the erodibility, and can therefore be used in estimating the erosion susceptibility. The soil texture affects the water's capacity to enter the soil and the infiltration rate. The results showed that 510.10 km² (28%) of the area was under very low severity, 742.33 km² (41%) under low, and 577.29 km² (32%) under medium severity. This was due to the major portion of study area being under the loam category of soil texture.

5. Conclusions

The analysis incorporated the GIS-based AHP to determine the distribution of critical areas with susceptibility to soil erosion in the Central Kashmir region. The AHP technique reduces bias in decision-making and provides an effective means to deal with multiple criteria and complex decisions. This framework is based on the effects of 11 different parameters developed from satellite images, geological, soil, and precipitation data. Five classes of severity were allocated based on the weighted sum analysis as very low–low (15% to 19%), medium (25%), and high–very high (27% to 14%). It was observed that almost all parameters selected in this study affected soil erosion in mountainous areas. However, the main effects can be seen from the topographical parameters in addition to LU_{LC} and lithology, followed by vegetation, moisture, precipitation, and soil types. From the analysis, it was perceived that the LU_{LC} and lithology covered 42% and 32% of the total area under the very high category of soil erosion susceptibility. The other conditioning parameters that covered the majority of the area under the very high soil erosion susceptibility class were aspect (19%), rainfall erosivity (18%), elevation, and slope (15%). The ND_{VI} and ND_{WI} also covered 16% and 15%, respectively, of the total area under consideration. Although the type of LU_{LC} and lithology underneath effects the soil erosion, at the same time, the aspect also contributes to soil erosion to a very large extent in mountainous terrain as the aspect controls the temperature, moisture, water supply, vegetation, and soil development. The main reason that triggers soil loss in the study area is due to the dearth of knowledge about agricultural practices on steep and high-altitude slopes. Aspect, drainage density, and curvature combined with lithology have a substantial effect on vulnerability to soil loss. The regions in the study area with high precipitation and wetness index are extremely erosive, aside from regions with barren land.

The results of the applied methodology have proven to be a very effective and timely method to qualitatively determine the suppressibility nature of erosion over a relatively large area. In this way, planners and policymakers can adopt this methodology for proper conservation measures. The present study contributes significantly to providing a useful prediction for decision-makers and the authorities in adopting appropriate approaches to minimize the potential damages that may occur due to soil erosion in the Sindh and Dachigam catchments. To minimize the degree of soil loss, the prerequisite is to examine the existing scientific management practices and develop appropriate conservative measures at the catchment level. The conservation strategies recommended include afforestation, tree plantation in urban areas, controlling excessive overgrazing, contour farming, developing a water conservation system, flood and erosion control systems, design of runoff water catchment systems, etc. While considering the control measures, one needs to consider the aspect factor as the slope orientation acts as a macro factor or integrating factor for the overall process of erosion. The conservation measures such as no-till (NT) practice can be carried out on agricultural land in which sowing is performed directly to stubble after preceding harvest without ploughing or other tillage practices typical for conventional tillage (CT), thus minimizing soil disturbance. Compared to conventional tillage, NT practice reduces the farm workload and has beneficial environmental impacts such as the effective reduction of erosion risk due to improved soil structure and continuous plant cover. Aside from helping to curtail soil loss, the procedures mentioned will also promote soil health and crop productivity, ultimately improving the livelihoods of people in the region.

Due to the uncertainties inherent in the conditioning factors, certain unreliability will always persist in soil erosion susceptibility assessments. The subjectivity of evaluation by experts may also have some limitations. Therefore, the fuzzy approach or machine learning algorithms can be considered in the future in addition to other significant conditioning factors such as spatiotemporal change of rainfall distribution and frequency under the climate change scenario.

Author Contributions: Conceptualization, F.M., M.F. and A.S.T.; Methodology, F.M. and M.F.; Software, F.M.; Validation, F.M.; Formal analysis, F.M.; Investigation, F.M.; Resources, M.F. and F.M.; Data

curation, F.M. and B.A.S.; Writing—original draft preparation, F.M., M.F. and A.S.T.; Writing—review and editing, F.M. and A.S.T.; Visualization, F.M. and M.F.; Supervision, M.F.; Project administration, M.F. and F.M. All authors have read and agreed to the published version of the manuscript.

Funding: No external funding was received for carrying out this study.

Institutional Review Board Statement: Not applicable.

Informed Consent Statement: Not applicable.

Data Availability Statement: Data shall be provided by the corresponding authors upon special request.

Acknowledgments: The authors are thankful to the four anonymous reviewers whose critical review has improved the quality of this manuscript. We are also thankful to the editor for their insightful comments that helped to provide the final shape to this manuscript. We acknowledge the support from the J&K State Remote Sensing Center for facilitating the data.

Conflicts of Interest: We hereby declare that there are conflicts of interest related to this submitted manuscript. The results presented here do not necessarily represent the views of the organizations the authors are associated with.

References

1. Boardman, J.; Poesen, J.; Evans, M. Slopes: Soil erosion. *Geol. Soc. Lond. Mem.* **2022**, *58*, 241–255. [[CrossRef](#)]
2. Borrelli, P.; Robinson, D.A.; Panagos, P.; Lugato, E.; Yang, J.E.; Alewell, C.; Ballabio, C. Land use and climate change impacts on global soil erosion by water (2015–2070). *Proc. Natl. Acad. Sci. USA* **2020**, *117*, 21994–22001. [[CrossRef](#)]
3. El-Swaify, S.A. Factors affecting soil erosion hazards and conservation needs for tropical steeplands. *Soil Technol.* **1997**, *11*, 3–16. [[CrossRef](#)]
4. Stoddart, D.R. World erosion and sedimentation. In *Introduction to Fluvial Processes*; Routledge: Oxfordshire, UK, 2019; pp. 8–29.
5. Comino, J.R.; Iserloh, T.; Lassu, T.; Cerdà, A.; Keestra, S.D.; Prosdocimi, M.; Ries, J.B. Quantitative comparison of initial soil erosion processes and runoff generation in Spanish and German vineyards. *Sci. Total Environ.* **2016**, *565*, 1165–1174. [[CrossRef](#)] [[PubMed](#)]
6. García-Ruiz, J.M.; Beguería, S.; Nadal-Romero, E.; González-Hidalgo, J.C.; Lana-Renault, N.; Sanjuán, Y. A meta-analysis of soil erosion rates across the world. *Geomorphology* **2015**, *239*, 160–173. [[CrossRef](#)]
7. Singh, G.; Babu, R.; Narain, P.; Bhushan, L.S.; Abrol, I.P. Soil erosion rates in India. *J. Soil Water Conserv.* **1992**, *47*, 97–99.
8. Raymo, M.E.; Ruddiman, W.F. Tectonic forcing of late Cenozoic climate. *Nature* **1992**, *359*, 117–122. [[CrossRef](#)]
9. Sandeep, P.; Reddy, G.O.; Jegankumar, R.; Kumar, K.A. Modeling and assessment of land degradation vulnerability in semi-arid ecosystem of Southern India using temporal satellite data, AHP and GIS. *Environ. Model. Assess.* **2021**, *26*, 143–154. [[CrossRef](#)]
10. Saini, S.S.; Jangra, R.; Kaushik, S.P. Vulnerability assessment of soil erosion using geospatial techniques-A pilot study of upper catchment of Markanda river. *Int. J. Adv. Remote Sens. GIS Geogr.* **2015**, *2*, 9–21.
11. Jain, S.K.; Kumar, S.; Varghese, J. Estimation of soil erosion for a Himalayan watershed using GIS technique. *Water Resour. Manag.* **2001**, *15*, 41–54. [[CrossRef](#)]
12. Wadia, D.N. *Geology of India*, 4th ed.; Tata McGraw-Hill Publishing Co.: New Delhi, India, 1979.
13. Pham, T.G.; Degener, J.; Kappas, M. Integrated universal soil loss equation (USLE) and Geographical Information System (GIS) for soil erosion estimation in A Sap basin: Central Vietnam. *Int. Soil Water Conserv. Res.* **2018**, *6*, 99–110. [[CrossRef](#)]
14. Williams, J.R. Sediment routing for agricultural watersheds. *JAWRA J. Am. Water Resour. Assoc.* **1975**, *11*, 965–974. [[CrossRef](#)]
15. Renard, K.G. *Predicting Soil Erosion by Water: A Guide to Conservation Planning with the Revised Universal Soil Loss Equation (RUSLE)*; United States Government Printing: Washington, DC, USA, 1997.
16. Alitane, A.; Essahlaoui, A.; El Hafyani, M.; El Hmaidi, A.; El Ouali, A.; Kassou, A.; Van Rompaey, A. Water Erosion Monitoring and Prediction in Response to the Effects of Climate Change Using RUSLE and SWAT Equations: Case of R'Dom Watershed in Morocco. *Land* **2022**, *11*, 93. [[CrossRef](#)]
17. Baigorria, G.A.; Romero, C.C. Assessment of erosion hotspots in a watershed: Integrating the WEPP model and GIS in a case study in the Peruvian Andes. *Environ. Model. Softw.* **2007**, *22*, 1175–1183. [[CrossRef](#)]
18. De Jong, S.M.; Paracchini, M.L.; Bertolo, F.; Folving, S.; Megier, J.; De Roo, A.P.J. Regional assessment of soil erosion using the distributed model SEMMED and remotely sensed data. *Catena* **1999**, *37*, 291–308. [[CrossRef](#)]
19. Grum, B.; Woldearegay, K.; Hessel, R.; Baartman, J.E.; Abdulkadir, M.; Yazew, E.; Geissen, V. Assessing the effect of water harvesting techniques on event-based hydrological responses and sediment yield at a catchment scale in northern Ethiopia using the Limburg Soil Erosion Model (LISEM). *Catena* **2017**, *159*, 20–34. [[CrossRef](#)]
20. Haregeweyn, N.; Yohannes, F. Testing and evaluation of the agricultural non-point source pollution model (AGNPS) on Augucho catchment, western Hararghe, Ethiopia. *Agric. Ecosyst. Environ.* **2003**, *99*, 201–212. [[CrossRef](#)]
21. Lu, D.; Li, G.; Valladares, G.S.; Batistella, M. Mapping soil erosion risk in Rondonia, Brazilian Amazonia: Using RUSLE, remote sensing and GIS. *Land Degrad. Dev.* **2004**, *15*, 499–512. [[CrossRef](#)]

22. Ouyang, W.; Hao, F.; Skidmore, A.K.; Toxopeus, A.G. Soil erosion and sediment yield and their relationships with vegetation cover in upper stream of the Yellow River. *Sci. Total Environ.* **2010**, *409*, 396–403. [[CrossRef](#)]
23. Veihe, A.; Rey, J.; Quinton, J.N.; Strauss, P.; Sancho, F.M.; Somarriba, M. Modelling of event-based soil erosion in Costa Rica, Nicaragua and Mexico: Evaluation of the EUROSEM model. *Catena* **2001**, *44*, 187–203. [[CrossRef](#)]
24. Mushtaq, F.; Lala, M.G.N.; Wadood, A. Estimation of soil erosion risk in upper catchment of Wular Lake, Jammu & Kashmir using RUSLE model. *Int. J. Adv. Res. Sci. Eng.* **2018**, *7*, 1828–1839.
25. Turkey, A.S.; Pandey, A.C.; Nathawat, M.S. Use of satellite data, GIS and RUSLE for estimation of average annual soil loss in Daltonganj watershed of Jharkhand (India). *J. Remote Sens. Technol.* **2013**, *1*, 20–30. [[CrossRef](#)]
26. Yüksel, A.; Akay, A.E.; Gundogan, R.; Reis, M.; Cetiner, M. Application of GeoWEPP for determining sediment yield and runoff in the Orcan Creek watershed in Kahramanmaraş, Turkey. *Sensors* **2008**, *8*, 1222–1236. [[CrossRef](#)]
27. Cerdà, A.; Borja, M.E.L.; Úbeda, X.; Martínez-Murillo, J.F.; Keesstra, S. *Pinus halepensis* M. versus *Quercus ilex* subsp. *Rotundifolia* L. runoff and soil erosion at pedon scale under natural rainfall in Eastern Spain three decades after a forest fire. *For. Ecol. Manag.* **2008**, *400*, 447–456. [[CrossRef](#)]
28. Eltner, A.; Mulsow, C.; Maas, H.G. Quantitative measurement of soil erosion from TLS and UAV data. *Int. Arch. Photogramm. Remote Sens. Spat. Inf. Sci.* **2013**, *40*, 4–6. [[CrossRef](#)]
29. Bosco, C.; de Rigo, D.; Dewitte, O.; Poesen, J.; Panagos, P. Modelling soil erosion at European scale: Towards harmonization and reproducibility. *Nat. Hazards Earth Syst. Sci.* **2015**, *15*, 225–245. [[CrossRef](#)]
30. Polidori, L.; El Hage, M. Digital elevation model quality assessment methods: A critical review. *Remote Sens.* **2020**, *12*, 3522. [[CrossRef](#)]
31. Borrelli, P.; Paustian, K.; Panagos, P.; Jones, A.; Schütt, B.; Lugato, E. Effect of good agricultural and environmental conditions on erosion and soil organic carbon balance: A national case study. *Land Use Policy* **2016**, *50*, 408–421. [[CrossRef](#)]
32. Prasuhn, V.; Liniger, H.; Gisler, S.; Herweg, K.; Candinas, A.; Clément, J.P. A high-resolution soil erosion risk map of Switzerland as strategic policy support system. *Land Use Policy* **2013**, *32*, 281–291. [[CrossRef](#)]
33. Al-Rahbi, A.K.H.; Abushammala, M.F.; Qazi, W.A. Application of the analytic hierarchy process for management of soil erosion in Oman. *Int. J. Anal. Hierarchy Process.* **2020**, *12*, 104–116. [[CrossRef](#)]
34. Aslam, B.; Maqsoom, A.; Alaloul, W.S.; Musarat, M.A.; Jabbar, T.; Zafar, A. Soil erosion susceptibility mapping using a GIS-based multi-criteria decision approach: Case of district Chitral, Pakistan. *Ain Shams Eng. J.* **2021**, *12*, 1637–1649. [[CrossRef](#)]
35. Chen, S.; Liu, W.; Bai, Y.; Luo, X.; Li, H.; Zha, X. Evaluation of watershed soil erosion hazard using combination weight and GIS: A case study from eroded soil in Southern China. *Nat. Hazards* **2021**, *109*, 1603–1628. [[CrossRef](#)]
36. Ni, J.R.; Li, X.X.; Borthwick, A.G.L. Soil erosion assessment based on minimum polygons in the Yellow River basin, China. *Geomorphology* **2008**, *93*, 233–252. [[CrossRef](#)]
37. Pradeep, G.S.; Krishnan, M.N.; Vijith, H. Identification of critical soil erosion prone areas and annual average soil loss in an upland agricultural watershed of Western Ghats, using analytical hierarchy process (AHP) and RUSLE techniques. *Arab. J. Geosci.* **2015**, *8*, 3697–3711. [[CrossRef](#)]
38. Rahman, M.R.; Shi, Z.H.; Chongfa, C. Soil erosion hazard evaluation—An integrated use of remote sensing, GIS and statistical approaches with biophysical parameters towards management strategies. *Ecol. Model.* **2009**, *220*, 1724–1734. [[CrossRef](#)]
39. Wu, Q.; Wang, M. A framework for risk assessment on soil erosion by water using an integrated and systematic approach. *J. Hydrol.* **2007**, *337*, 11–21. [[CrossRef](#)]
40. Agnihotri, D.; Kumar, T.; Jhariya, D. Intelligent vulnerability prediction of soil erosion hazard in semi-arid and humid region. *Environ. Dev. Sustain.* **2021**, *23*, 2524–2551. [[CrossRef](#)]
41. Singh, G.; Singh, R.M.; Singh, S.; Kumar, A.R.S.; Jaiswal, R.K.; Chandola, V.K.; Nema, A.K. Multi-criteria analytical hierarchical process based decision support system for critical watershed prioritization of Andhiyarkhore catchment. *Indian J. Soil Conserv.* **2019**, *47*, 263–272.
42. Pramanik, M.K. Site suitability analysis for agricultural land use of Darjeeling district using AHP and GIS techniques. *Model. Earth Syst. Environ.* **2016**, *2*, 1–22. [[CrossRef](#)]
43. Kundu, S.; Khare, D.; Mondal, A. Landuse change impact on sub-watersheds prioritization by analytical hierarchy process (AHP). *Ecol. Inform.* **2017**, *42*, 100–113. [[CrossRef](#)]
44. Oh, H.J.; Lee, S. Integration of ground subsidence hazard maps of abandoned coal mines in Samcheok, Korea. *Int. J. Coal Geol.* **2011**, *86*, 58–72. [[CrossRef](#)]
45. Kim, K.D.; Lee, S.; Oh, H.J.; Choi, J.K.; Won, J.S. Assessment of ground subsidence hazard near an abandoned underground coal mine using GIS. *Environ. Geol.* **2006**, *50*, 1183–1191. [[CrossRef](#)]
46. Lee, S.; Oh, H.J.; Kim, K.D. Statistical spatial modeling of ground subsidence hazard near an abandoned underground coal mine. *Disaster Adv.* **2010**, *3*, 11–12.
47. Pradhan, B.; Lee, S. Utilization of optical remote sensing data and GIS tools for regional landslide hazard analysis by using an artificial neural network model. *Earth Sci. Front.* **2007**, *14*, 143–152.
48. Yilmaz, I. A case study from Koyulhisar (Sivas-Turkey) for landslide susceptibility mapping by artificial neural networks. *Bull. Eng. Geol. Environ.* **2009**, *68*, 297–306. [[CrossRef](#)]
49. Choi, J.K.; Kim, K.D.; Lee, S.; Won, J.S. Application of a fuzzy operator to susceptibility estimations of coal mine subsidence in Taebaek City, Korea. *Environ. Earth Sci.* **2010**, *59*, 1009–1022. [[CrossRef](#)]

50. Ghafari, A.S.; Alasty, A. Design and real-time experimental implementation of gain scheduling PID fuzzy controller for hybrid stepper motor in micro-step operation. In Proceedings of the IEEE International Conference on Mechatronics, 2004, ICM'04, Istanbul, Turkey, 5 June 2004; IEEE: Piscataway, NJ, USA, 2004; pp. 421–426.
51. Tehrany, M.S.; Shabani, F.; Javier, D.N.; Kumar, L. Soil erosion susceptibility mapping for current and 2100 climate conditions using evidential belief function and frequency ratio. *Geomat. Nat. Hazards Risk* **2017**, *8*, 1695–1714. [[CrossRef](#)]
52. Kadavi, P.R.; Lee, C.W.; Lee, S. Application of ensemble-based machine learning models to landslide susceptibility mapping. *Remote Sens.* **2018**, *10*, 1252. [[CrossRef](#)]
53. Lee, S.; Pradhan, B. Probabilistic landslide hazards and risk mapping on Penang Island, Malaysia. *J. Earth Syst. Sci.* **2006**, *115*, 661–672. [[CrossRef](#)]
54. Costache, R.; Ngo, P.T.T.; Bui, D.T. Novel ensembles of deep learning neural network and statistical learning for flash-flood susceptibility mapping. *Water* **2020**, *12*, 1549. [[CrossRef](#)]
55. Ijlil, S.; Essahlaoui, A.; Mohajane, M.; Essahlaoui, N.; Mili, E.M.; Van Rompaey, A. Machine Learning Algorithms for Modeling and Mapping of Groundwater Pollution Risk: A Study to Reach Water Security and Sustainable Development (Sdg) Goals in a Mediterranean Aquifer System. *Remote Sens.* **2022**, *14*, 2379. [[CrossRef](#)]
56. Clerici, A.; Perego, S.; Tellini, C.; Vescovi, P. A procedure for landslide susceptibility zonation by the conditional analysis method. *Geomorphology* **2002**, *48*, 349–364. [[CrossRef](#)]
57. Scheet, P.; Stephens, M. A fast and flexible statistical model for large-scale population genotype data: Applications to inferring missing genotypes and haplotypic phase. *Am. J. Hum. Genet.* **2006**, *78*, 629–644. [[CrossRef](#)] [[PubMed](#)]
58. Zaz, S.N.; Romshoo, S.A. Assessing the geoinicators of land degradation in the Kashmir Himalayan region, India. *Nat. Hazards* **2012**, *64*, 1219–1245. [[CrossRef](#)]
59. Mosavi, A.; Sajedi-Hosseini, F.; Choubin, B.; Taramideh, F.; Rahi, G.; Dineva, A.A. Susceptibility mapping of soil water erosion using machine learning models. *Water* **2020**, *12*, 1995. [[CrossRef](#)]
60. Conoscenti, C.; Di Maggio, C.; Rotigliano, E. Soil erosion susceptibility assessment and validation using a geostatistical multivariate approach: A test in Southern Sicily. *Nat. Hazards* **2008**, *46*, 287–305. [[CrossRef](#)]
61. Halefom, A.; Teshome, A. Modelling and mapping of erosion potentiality watersheds using AHP and GIS technique: A case study of Alamata Watershed, South Tigray, Ethiopia. *Model. Earth Syst. Environ.* **2019**, *5*, 819–831. [[CrossRef](#)]
62. Rahmati, O.; Haghizadeh, A.; Pourghasemi, H.R.; Noormohamadi, F. Gully erosion susceptibility mapping: The role of GIS-based bivariate statistical models and their comparison. *Nat. Hazards* **2016**, *82*, 1231–1258. [[CrossRef](#)]
63. Zabihi, M.; Mircholi, F.; Motevalli, A.; Darvishan, A.K.; Pourghasemi, H.R.; Zakeri, M.A.; Sadighi, F. Spatial modelling of gully erosion in Mazandaran Province, northern Iran. *Catena* **2018**, *161*, 1–13. [[CrossRef](#)]
64. Yilmaz, C.; Topal, T.; Süzen, M.L. GIS-based landslide susceptibility mapping using bivariate statistical analysis in Devrek (Zonguldak-Turkey). *Environ. Earth Sci.* **2012**, *65*, 2161–2178. [[CrossRef](#)]
65. Blanco, H.; Lal, R. *Principles of Soil Conservation and Management*; Springer: New York, NY, USA, 2008; Volume 167169.
66. Jin, Z.; Zhao, Q.; Qin, X.; Zhang, J.; Zhang, H.; Qin, J.; Wang, L. Quantifying the impact of landscape changes on hydrological variables in the alpine and cold region using hydrological model and remote sensing data. *Hydrol. Process.* **2021**, *35*, e14392. [[CrossRef](#)]
67. Sarkar, S.; Kanungo, D.P. An integrated approach for landslide susceptibility mapping using remote sensing and GIS. *Photogramm. Eng. Remote Sens.* **2004**, *70*, 617–625. [[CrossRef](#)]
68. Nearing, M.A.; Yin, S.Q.; Borrelli, P.; Polyakov, V.O. Rainfall erosivity: An historical review. *Catena* **2017**, *157*, 357–362. [[CrossRef](#)]
69. Lee, J.H.; Heo, J.H. Evaluation of estimation methods for rainfall erosivity based on annual precipitation in Korea. *J. Hydrol.* **2011**, *409*, 30–48. [[CrossRef](#)]
70. Singh, G.; Babu, R.; Chandra, S. *Soil Loss Prediction Research in India*; Technical Bulletin T-12/D-9; Central Soil and Water Conservation Research and Training Institute: Dehradun, India, 1981.
71. Choudhury, M.K.; Nayak, T. Estimation of soil erosion in Sagar Lake catchment of Central India. In Proceedings of the International Conference on Water and Environment, Bhopal, India, 15–18 December 2003; Volume 15, pp. 387–392.
72. Kumar, A.; Devi, M.; Deshmukh, B. Integrated remote sensing and geographic information system-based RUSLE modelling for estimation of soil loss in western Himalaya, India. *Water Resour. Manag.* **2014**, *28*, 3307–3317. [[CrossRef](#)]
73. Mushtaq, F.; Lala, M.G.N. Assessment of hydrological response as a function of LULC change and climatic variability in the catchment of the Wular Lake, J&K, using geospatial technique. *Environ. Earth Sci.* **2017**, *76*, 1–19.
74. Conforti, M.; Aucelli, P.P.; Robustelli, G.; Scarciglia, F. Geomorphology and GIS analysis for mapping gully erosion susceptibility in the Turbolo stream catchment (Northern Calabria, Italy). *Nat. Hazards* **2011**, *56*, 881–898. [[CrossRef](#)]
75. Rhett, J.; Thompson, J.; Kolka, R. *Wetland Soils, Hydrology, and Geomorphology*; University of California Press: Berkeley, CA, USA, 2014.
76. Sánchez-Ruiz, S.; Piles, M.; Sánchez, N.; Martínez-Fernández, J.; Vall-llossera, M.; Camps, A. Combining SMOS with visible and near/shortwave/thermal infrared satellite data for high resolution soil moisture estimates. *J. Hydrol.* **2014**, *516*, 273–283. [[CrossRef](#)]
77. Saha, S.; Gayen, A.; Pourghasemi, H.R.; Tiefenbacher, J.P. Identification of soil erosion-susceptible areas using fuzzy logic and analytical hierarchy process modeling in an agricultural watershed of Burdwan district, India. *Environ. Earth Sci.* **2019**, *78*, 1–18. [[CrossRef](#)]
78. Wentworth, C.K. A simplified method of determining the average slope of land surfaces. *Am. J. Sci.* **1930**, *5*, 184–194. [[CrossRef](#)]

79. Horn, B.K. Hill shading and the reflectance map. *Proc. IEEE* **1981**, *69*, 14–47. [[CrossRef](#)]
80. Zevenbergen, L.W.; Thorne, C.R. Quantitative analysis of land surface topography. *Earth Surf. Process. Landf.* **1987**, *12*, 47–56. [[CrossRef](#)]
81. Wischmeier, W.H.; Johnson, C.B.; Cross, B.V. Soil erodibility nomograph for farmland and construction sites. *J. Soil Water Conserv.* **1971**, *26*, 5189.
82. Vogelmann, J.E.; Sohl, T.; Howard, S.M. Regional characterization of land cover using multiple sources of data. *Photogramm. Eng. Remote Sens.* **1998**, *64*, 45–57.
83. Pavelsky, T.M.; Smith, L.C. Remote sensing of hydrologic recharge in the Peace-Athabasca Delta, Canada. *Geophys. Res. Lett.* **2008**, *35*, 1–5. [[CrossRef](#)]
84. Mahmood, T.H.; Hasan, K.; Akhter, S.H. Lithologic mapping of a forested montane terrain from Landsat 5 TM image. *Geocarto Int.* **2019**, *34*, 750–768. [[CrossRef](#)]
85. McFeeters, S.K. The use of the Normalized Difference Water Index (NDWI) in the delineation of open water features. *Int. J. Remote Sens.* **1996**, *17*, 1425–1432. [[CrossRef](#)]
86. Tucker, C.J. Red and photographic infrared linear combinations for monitoring vegetation. *Remote Sens. Environ.* **1979**, *8*, 127–150. [[CrossRef](#)]
87. Uddin, K.; Abdul Matin, M.; Maharjan, S. Assessment of land cover change and its impact on changes in soil erosion risk in Nepal. *Sustainability* **2018**, *10*, 4715. [[CrossRef](#)]
88. Mirmousavi, S.H. Regional modeling of wind erosion in the North West and South West of Iran. *Eurasian Soil Sci.* **2016**, *49*, 942–953. [[CrossRef](#)]
89. Saaty, T.L. Basic theory of the analytic hierarchy process: How to make a decision. *Rev. Real Acad. Cienc. Exactas Fis. Nat.* **1999**, *93*, 395–423.
90. Kayastha, P.; Dhital, M.R.; De Smedt, F. Application of the analytical hierarchy process (AHP) for landslide susceptibility mapping: A case study from the Tinau watershed, west Nepal. *Comput. Geosci.* **2013**, *52*, 398–408. [[CrossRef](#)]
91. Saaty, T.L. The Analytic Hierarchy Process: Decision Making in Complex Environments. In *Quantitative Assessment in Arms Control*; Avenhaus, R., Huber, R.K., Eds.; Springer: Boston, MA, USA, 1984; pp. 285–308.
92. Saaty, T.L. Decision making—The analytic hierarchy and network processes (AHP/ANP). *J. Syst. Sci. Syst. Eng.* **2004**, *3*, 1–35. [[CrossRef](#)]
93. Pandey, A.; Mathur, A.; Mishra, S.K.; Mal, B.C. Soil erosion modeling of a Himalayan watershed using RS and GIS. *Environ. Earth Sci.* **2009**, *59*, 399–410. [[CrossRef](#)]
94. Jhariya, D.C.; Kumar, T.; Pandey, H.K. Watershed prioritization based on soil and water hazard model using remote sensing, geographical information system and multi-criteria decision analysis approach. *Geocarto Int.* **2020**, *35*, 188–208. [[CrossRef](#)]
95. Ashraf, A. Risk modeling of soil erosion under different land use and rainfall conditions in Soan river basin, sub-Himalayan region and mitigation options. *Model. Earth Syst. Environ.* **2020**, *6*, 417–428. [[CrossRef](#)]
96. Yesuph, A.Y.; Dagnew, A.B. Soil erosion mapping and severity analysis based on RUSLE model and local perception in the Beshillo Catchment of the Blue Nile Basin, Ethiopia. *Environ. Syst. Res.* **2019**, *8*, 1–21. [[CrossRef](#)]
97. Amin, M.; Romshoo, S.A. Comparative assessment of soil erosion modelling approaches in a Himalayan watershed. *Model. Earth Syst. Environ.* **2019**, *5*, 175–192. [[CrossRef](#)]
98. Mushi, C.A.; Ndomba, P.M.; Trigg, M.A.; Tshimanga, R.M.; Mtalo, F. Assessment of basin-scale soil erosion within the Congo River Basin: A review. *Catena* **2019**, *178*, 64–76. [[CrossRef](#)]
99. Kulimushi, L.C.; Choudhari, P.; Maniragaba, A.; Elbeltagi, A.; Mugabowindekwe, M.; Rwanyiziri, G.; Singh, S.K. Erosion risk assessment through prioritization of sub-watersheds in Nyabarongo river catchment, Rwanda. *Environ. Chall.* **2021**, *5*, 100260. [[CrossRef](#)]
100. Das, B.; Bordoloi, R.; Thungon, L.T.; Paul, A.; Pandey, P.K.; Mishra, M.; Tripathi, O.P. An integrated approach of GIS, RUSLE and AHP to model soil erosion in West Kameng watershed, Arunachal Pradesh. *J. Earth Syst. Sci.* **2020**, *129*, 1–18. [[CrossRef](#)]
101. Jaiswal, R.K.; Thomas, T.; Galkate, R.V.; Ghosh, N.C.; Singh, S. Watershed prioritization using Saaty's AHP based decision support for soil conservation measures. *Water Resour. Manag.* **2014**, *28*, 475–494. [[CrossRef](#)]
102. Bryan, R.B. Soil erodibility and processes of water erosion on hillslope. *Geomorphology* **2000**, *32*, 385–415. [[CrossRef](#)]
103. Mahalder, B.; Schwartz, J.S.; Palomino, A.M.; Zirkle, J. Relationships between physical-geochemical soil properties and erodibility of streambanks among different physiographic provinces of Tennessee, USA. *Earth Surf. Process. Landf.* **2018**, *43*, 401–416. [[CrossRef](#)]
104. Angulo-Martinez, M.; Beguería, S.; Navas, A.; Machin, J. Splash erosion under natural rainfall on three soil types in NE Spain. *Geomorphology* **2012**, *175*, 38–44. [[CrossRef](#)]
105. Saedi, T.; Shorafa, M.; Gorji, M.; Moghadam, B.K. Indirect and direct effects of soil properties on soil splash erosion rate in calcareous soils of the central Zagross, Iran: A laboratory study. *Geoderma* **2016**, *271*, 1–9. [[CrossRef](#)]
106. Cheng, Q.; Cai, Q.; Ma, W. Comparative study on rain splash erosion of representative soils in China. *Chin. Geogr. Sci.* **2008**, *18*, 155–161. [[CrossRef](#)]
107. Fernández-Raga, M.; Palencia, C.; Keesstra, S.; Jordán, A.; Fraile, R.; Angulo-Martínez, M.; Cerdà, A. Splash erosion: A review with unanswered questions. *Earth-Sci. Rev.* **2017**, *171*, 463–477. [[CrossRef](#)]

108. Fu, Y.; Li, G.L.; Zheng, T.H.; Li, B.Q.; Zhang, T. Splash detachment and transport of loess aggregate fragments by raindrop action. *Catena* **2017**, *150*, 154–160. [[CrossRef](#)]
109. ÓGeen, A.T.; Elkins, R.; Lewis, D. Division of Agriculture and Natural Resources. 2006. Available online: <https://ucanr.edu/> (accessed on 26 November 2022).
110. McDonald, M.A.; Healey, J.R.; Stevens, P.A. The effects of secondary forest clearance and subsequent land-use on erosion losses and soil properties in the Blue Mountains of Jamaica. *Agric. Ecosyst. Environ.* **2002**, *92*, 1–19. [[CrossRef](#)]
111. Chalise, D.; Kumar, L.; Shrivastav, C.P.; Lamichhane, S. Spatial assessment of soil erosion in a hilly watershed of Western Nepal. *Environ. Earth Sci.* **2018**, *77*, 685. [[CrossRef](#)]
112. Chapin, F.S.; Oechel, W.C.; Van Cleve, K.; Lawrence, W. The role of mosses in the phosphorus cycling of an Alaskan black spruce forest. *Oecologia* **1987**, *74*, 310–315. [[CrossRef](#)] [[PubMed](#)]
113. Kachouri, S.; Achour, H.; Abida, H.; Bouaziz, S. Soil erosion hazard mapping using Analytic Hierarchy Process and logistic regression: A case study of Haffouz watershed, central Tunisia. *Arab. J. Geosci.* **2015**, *8*, 4257–4268. [[CrossRef](#)]
114. Mahapatra, S.K.; Reddy, G.O.; Nagdev, R.; Yadav, R.P.; Singh, S.K.; Sharda, V.N. Assessment of soil erosion in the fragile Himalayan ecosystem of Uttarakhand, India using USLE and GIS for sustainable productivity. *Curr. Sci.* **2018**, *115*, 108–121. [[CrossRef](#)]
115. Yang, T.; Siddique, K.H.; Liu, K. Cropping systems in agriculture and their impact on soil health-A review. *Glob. Ecol. Conserv.* **2020**, *23*, e01118. [[CrossRef](#)]
116. Jaafari, A.; Najafi, A.; Pourghasemi, H.R.; Rezaeian, J.; Sattarian, A. GIS-based frequency ratio and index of entropy models for landslide susceptibility assessment in the Caspian forest, northern Iran. *Int. J. Environ. Sci. Technol.* **2014**, *11*, 909–926. [[CrossRef](#)]
117. Méndez-Toribio, M.; Meave, J.A.; Zermeño-Hernández, I.; Ibarra-Manríquez, G. Effects of slope aspect and topographic position on environmental variables, disturbance regime and tree community attributes in a seasonal tropical dry forest. *J. Veg. Sci.* **2016**, *27*, 1094–1103. [[CrossRef](#)]
118. Gallardo-Cruz, J.A.; Pérez-García, E.A.; Meave, J.A. β -Diversity and vegetation structure as influenced by slope aspect and altitude in a seasonally dry tropical landscape. *Landsc. Ecol.* **2009**, *24*, 473–482. [[CrossRef](#)]
119. Yang, Q.; Xie, Y.; Li, W.; Jiang, Z.; Li, H.; Qin, X. Assessing soil erosion risk in karst area using fuzzy modeling and method of the analytical hierarchy process. *Environ. Earth Sci.* **2014**, *71*, 287–292. [[CrossRef](#)]
120. George, K.J.; Kumar, S.; Hole, R.M. Geospatial modelling of soil erosion and risk assessment in Indian Himalayan region—A study of Uttarakhand state. *Environ. Adv.* **2021**, *4*, 100039. [[CrossRef](#)]
121. Makaya, N.; Dube, T.; Seutloali, K.; Shoko, C.; Mutanga, O.; Masocha, M. Geospatial assessment of soil erosion vulnerability in the upper uMgeni catchment in KwaZulu Natal, South Africa. *Phys. Chem. Earth Parts A/B/C* **2019**, *112*, 50–57. [[CrossRef](#)]
122. Seutloali, K.E.; Beckedahl, H.R. A review of road-related soil erosion: An assessment of causes, evaluation techniques and available control measures. *Earth Sci. Res. J.* **2015**, *19*, 73–80. [[CrossRef](#)]
123. McCloskey, J.T.; Lillieholm, R.J.; Cronan, C. Using Bayesian belief networks to identify potential compatibilities and conflicts between development and landscape conservation. *Landsc. Urban Plan.* **2011**, *101*, 190–203. [[CrossRef](#)]
124. Rather, M.A.; Satish Kumar, J.; Farooq, M.; Rashid, H. Assessing the influence of watershed characteristics on soil erosion susceptibility of Jhelum basin in Kashmir Himalayas. *Arab. J. Geosci.* **2017**, *10*, 1–25. [[CrossRef](#)]
125. Meraj, G.; Romshoo, S.A.; Yousuf, A.R. Geoinformatics approach to qualitative forest density loss estimation and protection cum conservation strategy—a case study of Pir Panjal range, J & K, India. *Int. J. Curr. Res. Rev.* **2012**, *4*, 47–61.
126. Romshoo, S.A.; Bhat, S.A.; Rashid, I. Geoinformatics for assessing the morphometric control on hydrological response at watershed scale in the Upper Indus Basin. *J. Earth Syst. Sci.* **2012**, *121*, 659–686. [[CrossRef](#)]
127. Saha, S. Geo-Environmental Evaluation for Exploring Potential Soil Erosion Areas of Jainti River Basin Using AHP Model, Eastern India. *Univers. J. Environ. Res. Technol.* **2018**, *7*, 38–55.
128. Gómez-Gutiérrez, Á.; Conoscenti, C.; Angileri, S.E.; Rotigliano, E.; Schnabel, S. Using topographical attributes to evaluate gully erosion proneness (susceptibility) in two mediterranean basins: Advantages and limitations. *Nat. Hazards* **2015**, *79*, 291–314. [[CrossRef](#)]

Disclaimer/Publisher's Note: The statements, opinions and data contained in all publications are solely those of the individual author(s) and contributor(s) and not of MDPI and/or the editor(s). MDPI and/or the editor(s) disclaim responsibility for any injury to people or property resulting from any ideas, methods, instructions or products referred to in the content.